NATIONAL INSTITUTE OF TECHNOLOGY TIRUCHIRAPPALLI
DPEARTMENT OF MECHANICAL ENGINEERING
Assignment - Group 6

Degree Program: B.Tech/M.Tech Course Code: MEPE11/ME606
Course Title: Computational Fluid Dynamics

Group Members:
211320013 MORE ROHAN APPASO
211320014 NAVNEET KUMAR SINGH
111118045 J KAILASH
111118047 KAJULURI GOWTHAM NAGA SAMEER REDDY

Q.1) Xie and Jian (Colloids and Surfaces A: Physicochem. Eng. Aspects 461 (2014) 231–239) studied the rotating electroosmotic flow of power-law fluids at high zeta potentials. Solve equations (12) and (13) from the paper numerically with appropriate boundary conditions. Compare the results from your numerical code with the results from the paper graphically. What are the inferences from your results?

Colloids and Surfaces A: Physicochem. Eng. Aspects 461 (2014) 231–239

Contents lists available at ScienceDirect

Colloids and Surfaces A: Physicochemical and Engineering Aspects

journal homepage: www.elsevier.com/locate/colsurfa

Rotating electroosmotic flow of power-law fluids at high zeta potentials

Zhi-Yong Xie, Yong-Jun Jian*

School of Mathematical Science, Inner Mongolia University, Hohhot, Inner Mongolia 010021, PR China

HIGHLIGHTS

- Rotating EOF of power-law fluids at high zeta potentials is analyzed.
- Finite difference method is used to compute rotating EOF velocity.
- The influences of dimensionless parameters on the velocity profiles are discussed.

GRAPHICAL ABSTRACT

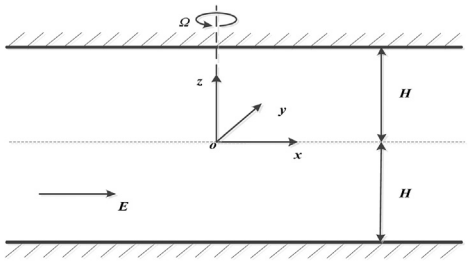

ARTICLE INFO

Article history:
Received 12 June 2014
Received in revised form 18 July 2014
Accepted 23 July 2014
Available online 10 August 2014

Keywords:
Rotating flow
Electroosmotic flow (EOF)
Electric double layer (EDL)
Power-law fluid
High zeta potentials
Finite difference method

ABSTRACT

In this paper, rotating electroosmotic flow (EOF) of power-law fluids at high zeta potentials in a slit microchannel is analyzed. The electric double layer (EDL) potential distribution is considered by using nonlinear Poisson–Boltzmann equation. Based upon the analytical charge density distribution, the finite difference method is used to compute numerically rotating EOF velocity profiles of power-law fluids. Results of the present analysis are compared with a simplified analysis obtained by Debye–Hückel linear approximation when the fluid is Newtonian. The classical steady plug-shape EOF velocity of non-Newtonian fluid is reduced for large enough time if the rotating effect is ignored. Additionally, the influences of the flow behavior index n, the rotating angular velocity Ω, wall Zeta potential ψ_w and the electrodynamic width K on the velocity profiles are discussed in detail.

1. Introduction

Recently, microfluidic devices have been greatly applied in micro-electromechanic system (MEMS) and microbiological sensors. Advanced microfluidic devices can perform complete biochemical analysis in a single fabricated chip [1,2]. Since the exchange of charges in channel wall and electrolyte, the free ions are either attracted to or repelled from a charged surface depending on the sign of the surface charges. Such a redistribution of free ions together with the surface ions gives rise to electric double layer (EDL). Electroosmotic flow (EOF) is the flow induced by the application of electric field across the channel and due to the presence of EDL at the channel wall [3]. In the field of microfluidics, the EOF attracts much research attention of the scholars due to many operational advantages, such as a plug-like velocity, negligible axial dispersion and better flow control.

Extensive studies of EOF have been investigated in microchannels with different shapes. Burgreen and Nakache [4] analyzed EOF in a parallel-plate channels. Cylindrical-shaped channels have been studied by Levine et al. [5]. Rice and White [6] have also studied the electrokinetic flow in a narrow cylindrical capillary. Tsao [7], Kang et al. [8] and Jian et al. [9] have reported the EOF flow in

* Corresponding author. Tel.: +86 471 4991251 8313; fax: +86 471 4991650.
E-mail address: jianyj@imu.edu.cn (Y.-J. Jian).

http://dx.doi.org/10.1016/j.colsurfa.2014.07.051
0927-7757/

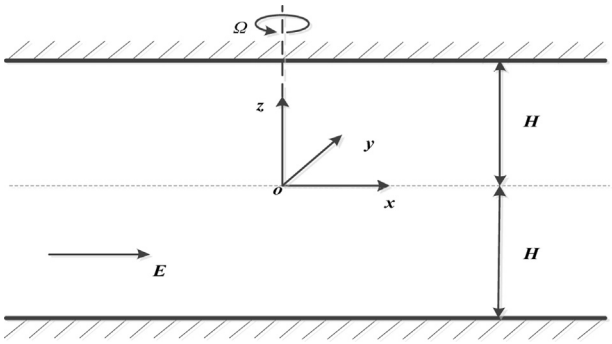

Fig. 1. Schematic of rotating EOF between two infinite microparallel plates.

annulus. Rectangular microchannel has been studied by Yang and Li [10], Yang et al. [11] and Arulanandam and Li [12]. However, rotating flow is a classical subject and there are many works about the rotating effects in geophysical fluid dynamics [13,14]. Hopfinger and Linden [15] reported the effects of background rotation on fluid motions under multifarious physical conditions. In practice, the microfluidic system may be located in a rotating environment, such as in centrifuges for flow control or mass separation.

A good advantage of using a centrifuge is that the centrifugal pump can dispel bubbles of gas in the microfluidic network. Duffy et al. [16] conducted experimental investigation of centrifugal microfluidic systems for electrokinetic control of liquid flow in multiple enzymatic assays. They found the centrifugation may relieve the problem of Joule heating. In addition, there are several literatures associated with the effect of uniform rotation on the electrohydrodynamic instability due to the theoretical importance. Takashima [17] first considered the effect of rotation on the onset of instability in a dielectric fluid layer under the action of a vertical ac electric field and a vertical temperature gradient. He found the Coriolis force has an inhibiting effect on the onset of instability. Othman [18] studied the electrohydrodynamic instability in a rotating viscoelastic dielectric fluid layer with heating effect from below. Ruo et al. [19] studied the effect of rotation on the electrohydrodynamic instability of a fluid layer with an electrical conductivity gradient. Recently, the rotating EOF between two plates was studied theoretically by Chang and Wang [20] under low zeta potential. They obtained analytical solutions of rotating EOF velocity and volume flow rate.

In most of the works, electrostatic potential distribution of EDL in microchannel is obtained by solving Poisson–Boltzmann

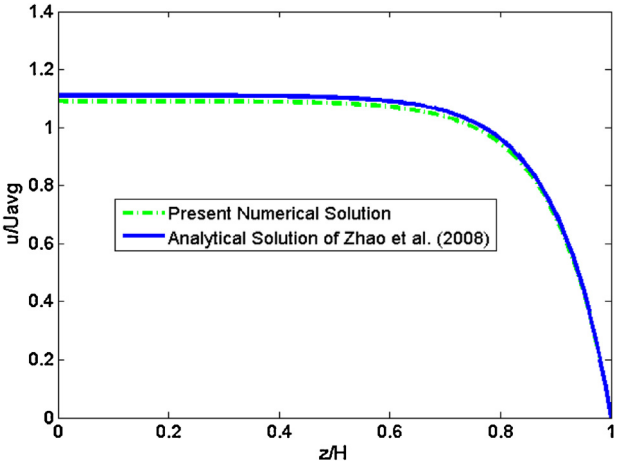

Fig. 3. Comparison of analytical solution in Ref. [32] with present numerical solution of the dimensionless rotating EOF velocity for $n = 1$ ($K = 10$, $\Omega = 0$ rad/s, $\psi_w = -0.025$ V).

equation with Debye–Hückel linear approximation. Their analysis is valid only for situations where the zeta potentials are sufficiently low. Hence, it is extremely realistic to have zeta potential and in such cases Debye–Hückel approximation fails to provide accurate electrostatic potential distribution. Dutta [21] studied transport of charged samples with large zeta potential, and he found the high zeta potential could facilitate transport. Kirby and Hasselbrink [22,23] studied the microfluidic substrates with high zeta potential, and they observed the effects on separation of species. Elazhary and Soliman [24] investigated the fluids of parallel-plate microchannel with high zeta potential and analyzed the heat transfer. Dutta and Beskok [25] studied the combined electroosmotic and pressure driven flows in microchannel with high zeta potential. Luo et al. [26] and Chun [27] have reported the secondary flow of EOF in a curved tube under high zeta potential. All the aforementioned research works are confined to Newtonian fluids.

However, microfluidic devices are often used to analyze biofluids, which are always non-Newtonian in nature. The main characteristic of non-Newtonian fluids is that the shear stress is not a linear function of the rate of strain tensor. Liu et al. [28,29] studied the EOF of Jeffrey fluid and generalized Maxwell fluid in a slit microchannel plate. Jian et al. [30] investigated the EOF of generalized Maxwell in a rectangular duct. Das and Chakraborty

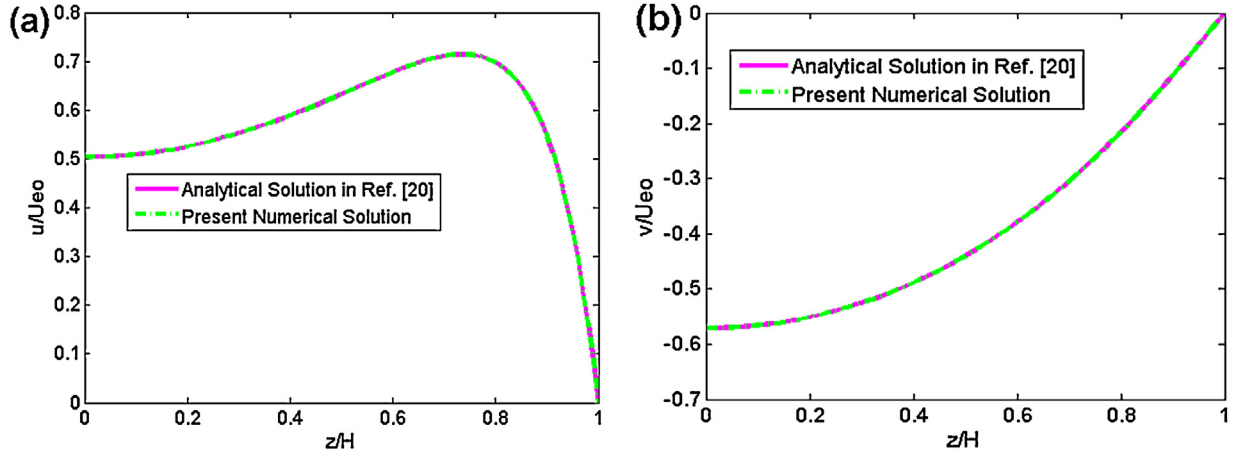

Fig. 2. Comparison of analytical solution in Ref. [20] with present numerical solution of the dimensionless rotating EOF velocity for $n = 1$ ($K = 10$, $\Omega = 100$ rad/s, $\psi_w = -0.025$ V). (a) Dimensionless velocity u in x direction. (b) Dimensionless velocity v in y direction.

Table 1
Comparison of analytical solutions in Ref. [20] with present numerical solutions.

u/U_{eo}				v/U_{eo}			
z/H	Analytical solution (u_A)	Present numerical solution (u_N)	Relative error $\lvert(u_A-u_N)/u_A\rvert$	z/H	Analytical solution (v_A)	Present numerical solution (v_N)	Relative error $\lvert(v_A-v_N)/v_A\rvert$
0	0.5041	0.5041	4.124e−5	0	−0.5707	−0.5707	4.106e−5
0.1	0.5092	0.5092	4.124e−5	0.1	−0.5661	−0.5661	4.106e−5
0.2	0.5092	0.5092	4.123e−5	0.2	−0.5512	−0.5512	4.106e−5
0.3	0.5524	0.5524	4.122e−5	0.3	−0.5258	−0.5258	4.105e−5
0.4	0.5889	0.5888	4.119e−5	0.4	−0.4891	−0.4891	4.103e−5
0.5	0.6325	0.6324	4.115e−5	0.5	−0.4406	−0.4406	4.101e−5
0.6	0.6777	0.6776	4.106e−5	0.6	−0.3795	−0.3795	4.098e−5
0.7	0.7110	0.7109	4.084e−5	0.7	−0.3047	−0.3047	4.094e−5
0.8	0.6974	0.6974	4.025e−5	0.8	−0.2157	−0.2157	4.086e−5
0.9	0.5441	0.5441	3.833e−5	0.9	−0.1130	−0.1130	4.075e−5
1	0	0	0	1	0	0	0

[31] analyzed the steady EOF of power-law fluids in microchannel within an approximation of hyperbolic sine function. The same fluid model is used to the study of steady EOF in slit microchannel by Zhao et al. [32]. Vasu and De [33] reported the EOF of power-law fluids with high zeta potential.

This study reports the rotating EOF of power-law fluids between two microparallel plates. The Navier–Stokes equations can be modified based on the constitution relation of power-law fluid in the rotating environment. By using the finite difference method, we obtained the velocity profile for various flow behavior index n. We find the numerical solution in steady status can be in good agreement with the exact solution reported by Chang and Wang [20] when the potential is low and the flow behavior index $n=1$. Furthermore, to ensure accuracy of the numerical solution, the result is compared with analytical results presented by Zhao et al. [32] under Debye–Hückel approximation and no rotating situation. Furthermore, the numerical solutions of the velocity profiles of rotating EOF of power-law fluids are computed for different behavior index n and the rotating angular velocity.

2. Model description

The rotating EOF of power-law fluid between two microparallel plates is sketched in Fig. 1. The height of the channel is $2H$. Let Cartesian coordinate (x, y, z) be placed at the midpoint of the channel. The y axis is pointing toward the inside of the plane and z axis is vertical to both plates. The entire system is rotating about the z axis. In a horizontal rotating fluid layer, all the velocity is relative velocity and is considered in non-inertial frame of reference. For an incompressible fluid, the continuity equation is given

$$\nabla \cdot \mathbf{V} = 0 \tag{1}$$

where $\mathbf{V}$ is the velocity of EOF. In a rotating system with constant angular velocity Ω, the Cauchy momentum equation is expressed as

$$\rho\left(\frac{\partial \mathbf{V}}{\partial t} + \mathbf{V}\cdot\nabla\mathbf{V} + 2\Omega\times\mathbf{V}\right) = -\nabla P + \nabla\cdot\boldsymbol{\tau} + \mathbf{F} \tag{2}$$

where ρ is the fluid density, t is the time, P is the pressure modified by centrifugal force, i.e., $P = p - \rho|\boldsymbol{\Omega}\times\mathbf{r}|^2/2$ with $\mathbf{r}=(x, y, z)$ and p is pressure. $\mathbf{F}$ is the body force vector, $\boldsymbol{\tau}$ is the stress tensor. In the present work, the power-law fluid is assumed and its dynamic viscosity μ is defined by Bird et al. [34]

$$\mu = \eta\Delta^{n-1} \tag{3}$$

where η is the consistency index, and n is the flow behavior index. Pseudoplastic fluid, namely $n<1$, often behave shear-thinning. Shear-thickening also termed as dilatant fluid behavior is obtained for $n>1$. Newtonian behavior is obtained for $n=1$. Δ is the magnitude of the rate of strain tensor and is defined as [34].

$$\Delta = \left[\frac{1}{2}(\boldsymbol{\Gamma}:\boldsymbol{\Gamma})\right]^{1/2} \tag{4}$$

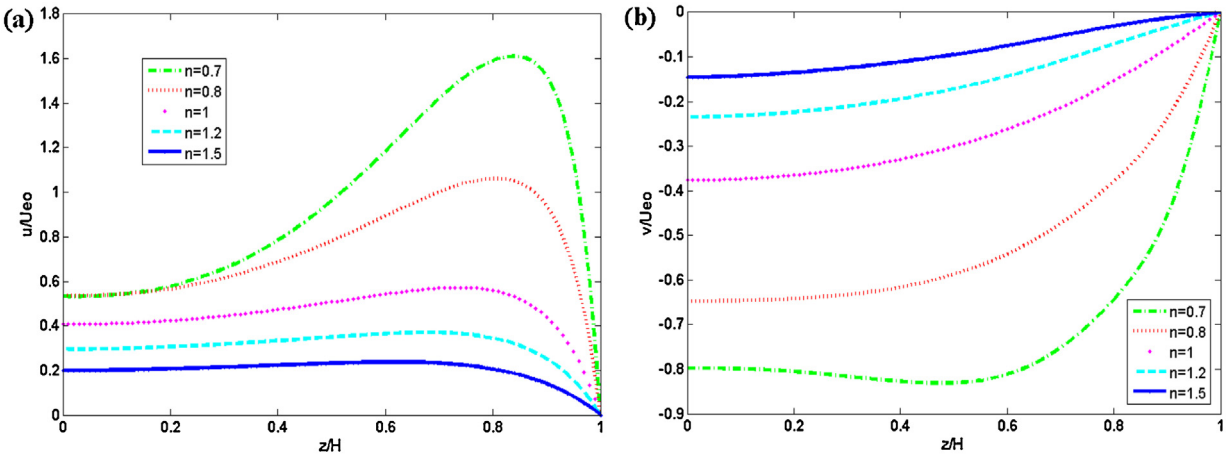

Fig. 4. The influence of power-law behavior index n on the rotating EOF velocity ($K=10$, $\Omega=100$ rad/s, $\psi_w=-0.1$ V). (a) Dimensionless velocity u in x direction. (b) Dimensionless velocity v in y direction.

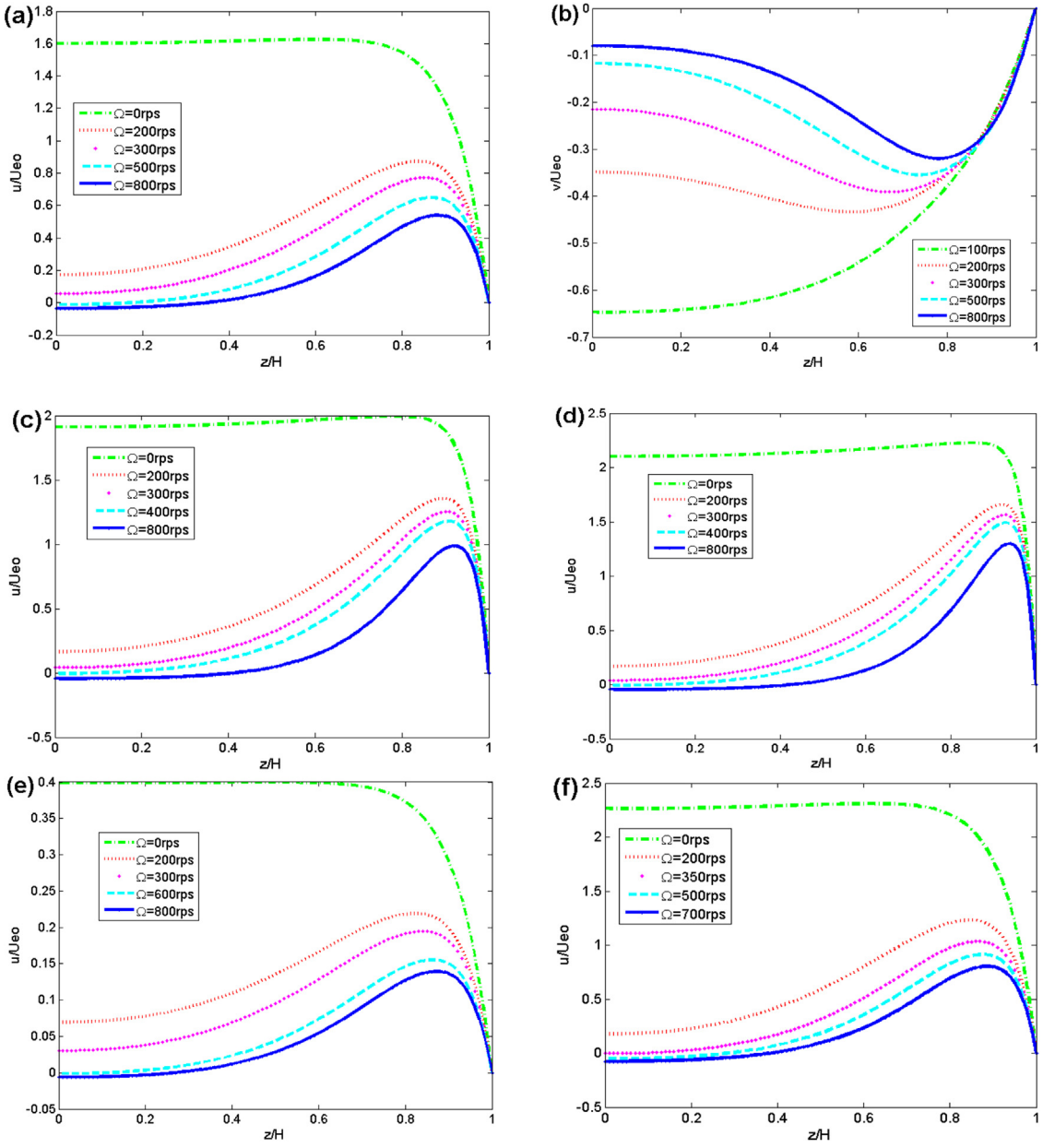

Fig. 5. The effect of the rotating angular velocity Ω on dimensionless EOF velocity ($n = 0.8$). (a) u in x direction ($K = 10$, $\psi_w = -0.1\,V$). (b) v in y direction ($K = 10$, $\psi_w = -0.1\,V$). (c) u in x direction ($K = 20$, $\psi_w = -0.1\,V$). (d) u in x direction ($K = 30$, $\psi_w = -0.1\,V$). (e) u in x direction ($K = 10$, $\psi_w = -0.025\,V$). (f) u in x direction ($K = 10$, $\psi_w = -0.25\,V$).

where $\boldsymbol{\Gamma}$ is the rate of strain tensor. In general, there is a relationship between the viscous stress tensor and the rate of strain tensor

$$\boldsymbol{\tau} = \mu(\Delta)[\nabla \mathbf{V} + (\nabla \mathbf{V})^T] \tag{5}$$

where $\nabla \mathbf{V}$ is the velocity gradient tensor and $(\nabla \mathbf{V})^T$ is its transpose.

In this study, the channel is filled with a liquid electrolyte of dielectric constant ε. We suppose that the system rotates about the z direction with $\boldsymbol{\Omega} = (0, 0, \Omega)$ and the EOF velocity is parallel to the plate $\mathbf{V} = (u, v, 0)$. Furthermore, for rotating EOF, it is assumed that the slit wall is uniformly charged with a zeta potential ψ_w, and there is no gravitational force and the modified pressure gradient in the flow field. Rotational effect appears only in terms of a Coriolis force, i.e., the last term on the left-hand side of Eq. (2). Thus the only external force is electrical field force at the right hand of Eq. (2). The electric field strength $\mathbf{E}$ is along x direction, namely $\mathbf{E} = (E, 0, 0)$. Because of symmetry, the analysis is restricted in the upper half domain of the slit microchannel. For binary symmetric electrolyte solution, the Poisson–Boltzmann equation of electrical potential gives

$$\frac{\mathrm{d}^2\psi}{\mathrm{d}z^2} = \frac{2z_0 e n_0}{\varepsilon} \sinh\left(\frac{z_0 e \psi}{k_b T}\right) \tag{6}$$

where n_0 is the ion density of bulk liquid, z_0 is the valence, e is the electron charge, k_b is the Boltzmann constant, and T is the absolute temperature.

The boundary conditions of Eq. (6) are

$$\text{At } z = H, \quad \psi = \psi_w \tag{7}$$

$$\text{At } z = 0, \quad \frac{\mathrm{d}\psi}{\mathrm{d}z} = 0 \tag{8}$$

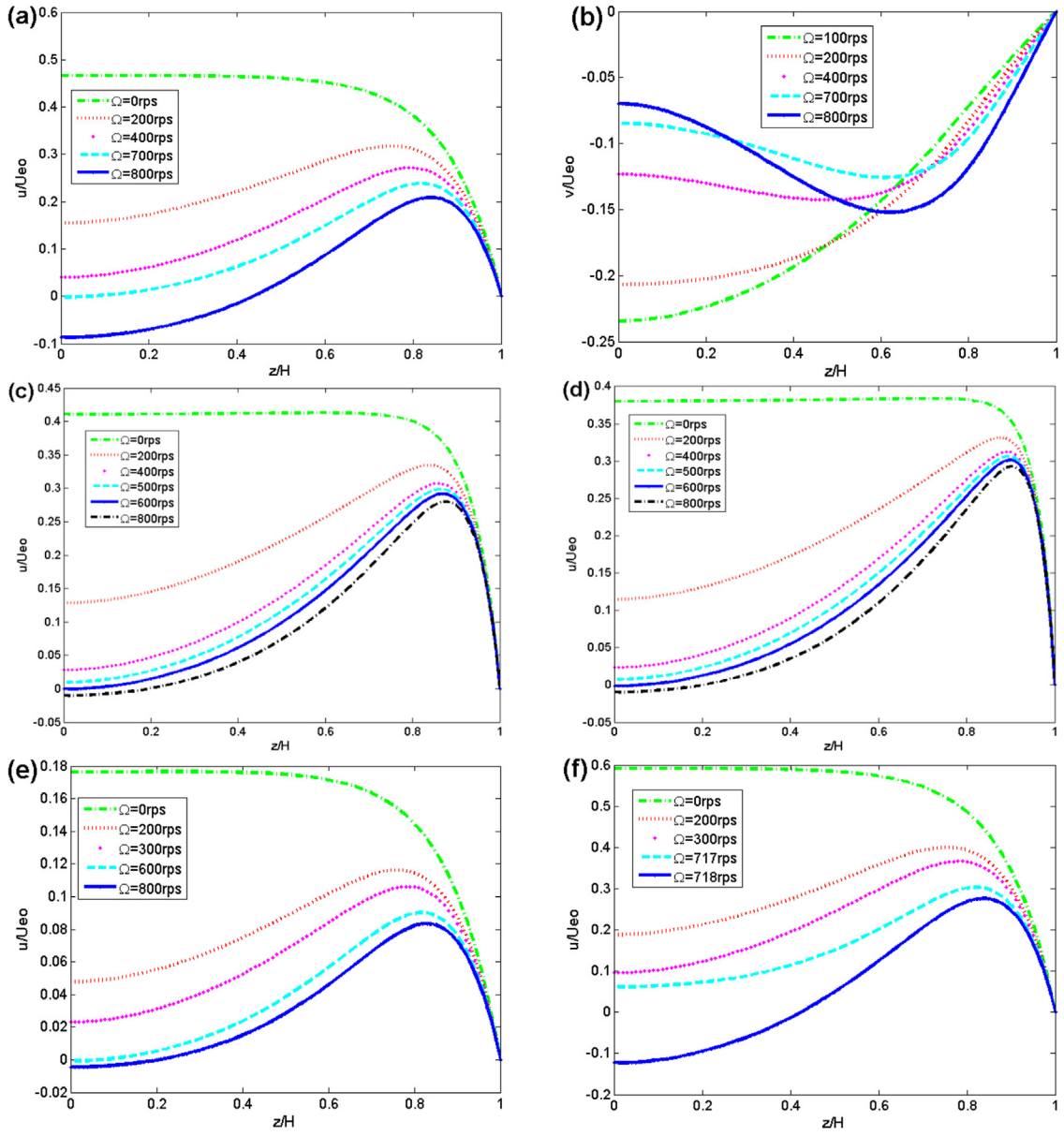

Fig. 6. The effect of the rotating angular velocity Ω on dimensionless EOF velocity ($n = 1.2$). (a) u in x direction ($K = 10$, $\psi_w = -0.1\,V$). (b) v in y direction ($K = 10$, $\psi_w = -0.1\,V$). (c) u in x direction ($K = 20$, $\psi_w = -0.1\,V$). (d) u in x direction ($K = 30$, $\psi_w = -0.1\,V$). (e) u in x direction ($K = 10$, $\psi_w = -0.025\,V$). (f) u in x direction ($K = 10$, $\psi_w = -0.25\,V$).

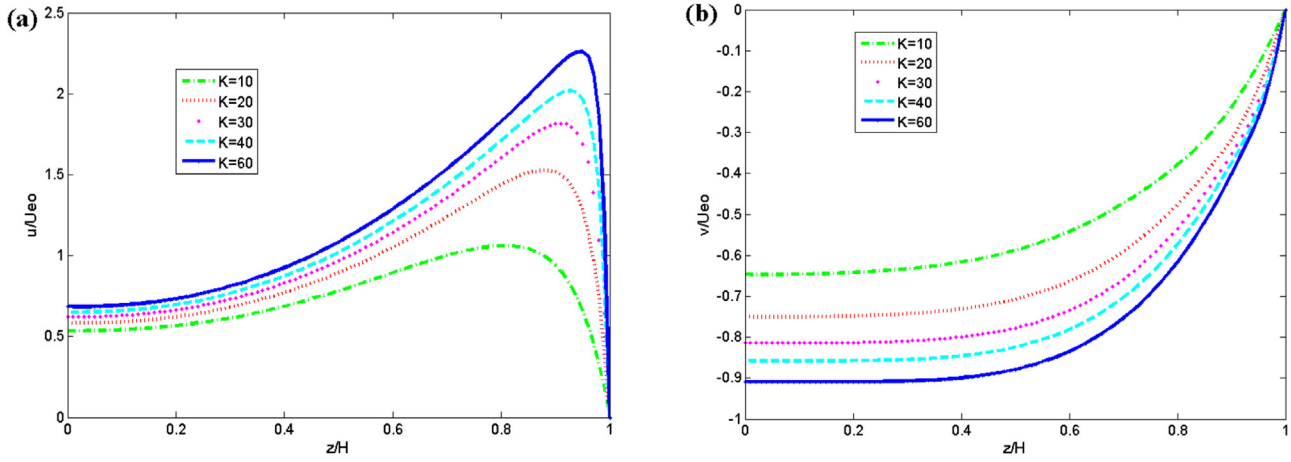

Fig. 7. The variations of the rotating EOF velocity with K ($n = 0.8$, $\Omega = 100$ rad/s, $\psi_w = -0.1\,V$). (a) Dimensionless velocity u in x direction. (b) Dimensionless velocity v in y direction.

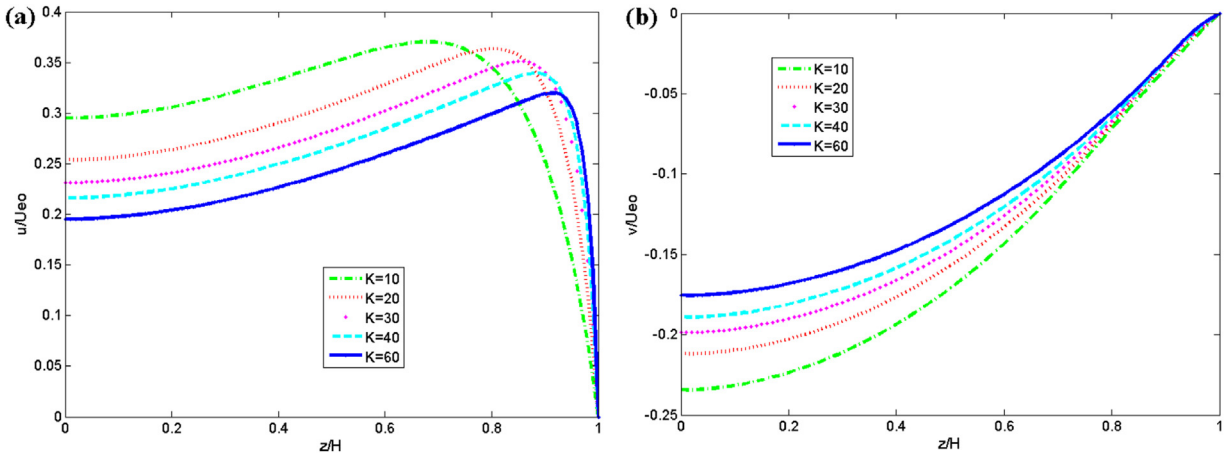

Fig. 8. The variations of the rotating EOF velocity with K ($n = 1.2$, $\Omega = 100$ rad/s, $\psi_w = -0.1$ V). (a) Dimensionless velocity u in x direction. (b) Dimensionless velocity v in y direction.

The solution to Eq. (6) subject to the boundary conditions of Eqs. (7) and (8) is given as [35]:

$$\psi = \frac{4\psi_w}{\alpha}\tanh^{-1}\left[\tanh\left(\frac{\alpha}{4}\right)\exp(\kappa z - \kappa H)\right] \tag{9}$$

where $\alpha = ze\psi_w/k_bT$ and $\kappa^2 = 2n_0z_2e_2/\varepsilon k_bT$, κ is the inverse double layer thickness.

Similar to the work of Chang and Wang [20], we may seek the solution $u = u(z,t)$, $v = v(z,t)$. In this case, the continuity Eq. (1) will be satisfied automatically. The viscous stress tensor can be simplified to

$$\mu(\Delta) = \eta\left[\left(\frac{\partial u}{\partial z}\right)^2 + \left(\frac{\partial v}{\partial z}\right)^2\right]^{(n-1)/2} \tag{10}$$

The shear stress can be written as

$$\tau_{zx} = \mu(\Delta)\frac{\partial u}{\partial z} \tag{11a}$$

$$\tau_{zy} = \mu(\Delta)\frac{\partial v}{\partial z} \tag{11b}$$

Therefore, the moment equations can be simplified to

$$\rho\left(\frac{\partial u}{\partial t} - 2\Omega v\right) = \frac{\partial}{\partial z}\left[\mu(\Delta)\frac{\partial u}{\partial z}\right] - \varepsilon\kappa^2 E\psi \tag{12}$$

$$\rho\left(\frac{\partial v}{\partial t} + 2\Omega u\right) = \frac{\partial}{\partial z}\left[\mu(\Delta)\frac{\partial v}{\partial z}\right] \tag{13}$$

Related initial and boundary conditions are

$$\text{At } t = 0, \quad u = v = 0 \tag{14}$$

$$\text{At } z = H, \quad u = v = 0 \tag{15}$$

$$\text{At } z = 0, \quad \frac{\partial u}{\partial z} = \frac{\partial v}{\partial z} = 0 \tag{16}$$

Particularly, $n = 1$ for $\mu(\Delta)$ in Eqs. (12) and (13) represents a Newtonian fluids flow driven by EOF under the rotating environment.

3. Numerical algorithm

We exploit symmetry about the z axis to consider the domain (t, z) belongs to $[0, T] \times [0, H]$, and discretize this domain by introducing grid points

$$t_m = m\Delta t, \quad m = 1, 2, \ldots, N_t \tag{17a}$$

$$z_i = i\Delta z, \quad i = 1, 2, 3, \ldots, N \tag{17b}$$

for grid spacings $\Delta t = T/(N_t - 1)$ and $\Delta z = H/(N - 1)$ in t and z direction, respectively. We index the variables u and v as follows:

$$u_i^m = u(t_m, z_i) \tag{18a}$$

$$v_i^m = v(t_m, z_i) \tag{18b}$$

A central finite difference scheme for Eq. (10) yields

$$\mu_i^m = \eta\left[\left(\frac{u_{i+1}^m - u_{i-1}^m}{2\Delta z}\right)^2 + \left(\frac{v_{i+1}^m - v_{i-1}^m}{2\Delta z}\right)^2\right]^{(n-1)/2} \tag{19}$$

Eqs. (12) and (13) are parabolic equations, forward differences in time derivatives are expressed as

$$\frac{\partial u}{\partial t} = \frac{u_i^{m+1} - u_i^m}{\Delta t} \tag{20a}$$

$$\frac{\partial v}{\partial t} = \frac{v_i^{m+1} - v_i^m}{\Delta t} \tag{20b}$$

Regarding the viscous terms of Eqs. (12) and (13), the algorithms of first forward difference and then backward difference are

$$\frac{\partial}{\partial z}\left(\mu\frac{\partial u}{\partial z}\right) = \frac{\mu_{i+1}^m\left(\frac{u_{i+1}^m - u_i^m}{\Delta z}\right) - \mu_i^m\left(\frac{u_i^m - u_{i-1}^m}{\Delta z}\right)}{\Delta z} \tag{21a}$$

$$\frac{\partial}{\partial z}\left(\mu\frac{\partial v}{\partial z}\right) = \frac{\mu_{i+1}^m\left(\frac{v_{i+1}^m - v_i^m}{\Delta z}\right) - \mu_i^m\left(\frac{v_i^m - v_{i-1}^m}{\Delta z}\right)}{\Delta z} \tag{21b}$$

The final differential equations of (12) and (13) become

$$\rho\left(\frac{u_i^{m+1} - u_i^m}{\Delta t}\right) = 2\rho\Omega v_i^m + \left[\mu_{i+1}^m\left(\frac{u_{i+1}^m - u_i^m}{\Delta z^2}\right) - \mu_i^m\left(\frac{u_i^m - u_{i-1}^m}{\Delta z^2}\right)\right] - \varepsilon E\kappa^2\psi_i \tag{22}$$

$$\rho\left(\frac{v_i^{m+1} - v_i^m}{\Delta t}\right) = -2\rho\Omega u_i^m + \left[\mu_{i+1}^m\left(\frac{v_{i+1}^m - v_i^m}{\Delta z^2}\right) - \mu_i^m\left(\frac{v_i^m - v_{i-1}^m}{\Delta z^2}\right)\right] \tag{23}$$

The corresponding initial and boundary conditions are

$$u_i^1 = 0, \quad v_i^1 = 0 \tag{24}$$

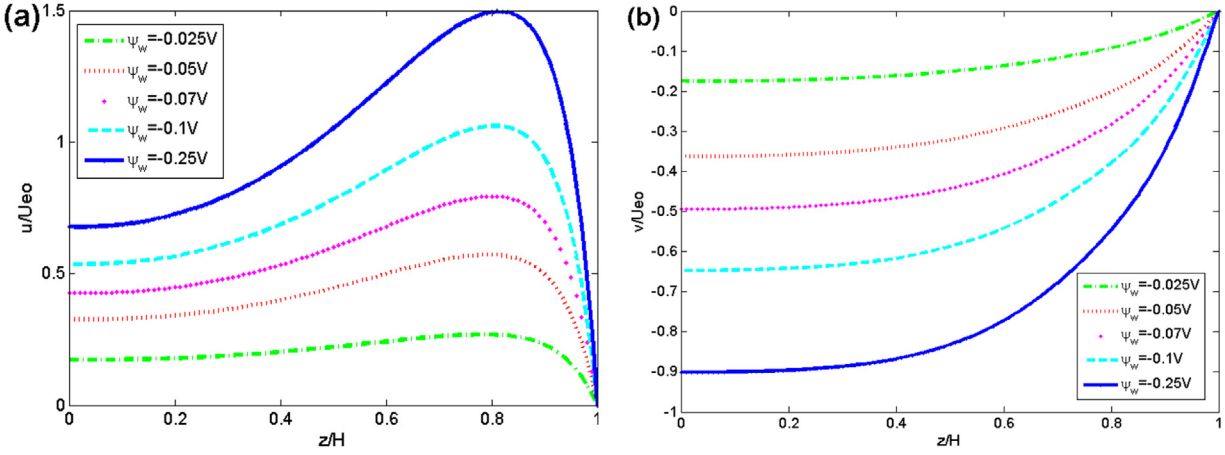

Fig. 9. The variations of the rotating EOF velocity with zeta potential, ψ_w ($n = 0.8$, $\Omega = 100$ rad/s, $K = 10$). (a) Dimensionless velocity u in x direction. (b) Dimensionless velocity v in y direction.

$$u_N^m = 0, \quad v_N^m = 0 \tag{25}$$

$$u_1^m = u_2^m, \quad v_1^m = v_2^m \tag{26}$$

Due to the fact that viscosity of the fluid depends on the velocity gradients, Eqs. (22) and (23) are obviously nonlinear and coupling parabolic equations and they can be computed numerically by using an iterative procedure of time. Besides, initial and boundary conditions are made for the viscosity at each grid point. The difference scheme we constructed is explicit and condition stable is evaluated approximately by $\left|\eta\Delta t/(\rho\Delta z^{n+1})\right| \leq 0.5$ with the special case when $n = 1$ for Newtonian fluid. Present work studies the microfluidics and all parameters are dimensional, thus small enough spatial and time steps are demanded and they are set to $\Delta z = 10^{-6}$ and $\Delta t = 5 \times 10^{-8}$, respectively in our computation. Three adjacent known points of u and three adjacent known points of v in present time step are used to compute the unknown velocity value in next time step point by point. This procedure is repeated until the relative error of $\left|(u_i^{m+1} - u_i^m)/u_i^{m+1}\right| \leq 10^{-9}$ between the present time step and the next time step at each spatial point is reached.

4. Results and discussion

In present calculations, the parametric values are taken as followings in typical microchannel flow. The permittivity of the electrolyte solution $\varepsilon = 709 \times 10^{-12}$ F/m, the half-height $H = 100$ μm, the electric field strength $E = 10^4$ V/m, the absolute temperature $T = 293$ K, the valence of ions $z_0 = 1$, the wall electrical potential $\psi_w = -0.1$ V, the flow consistency, $\eta = 0.9 \times 10^{-3}$ Pa s^n, the concentration of electrolyte solution $n_0 = N_A c$, c is the molar concentration and $c = 10^{-5}$ mol/L, $N_A = 6.02 \times 10^{23}$/mol, $e = 1.6 \times 10^{-19}$ C, $k_b = 1.38 \times 10^{-23}$ J/K and $\rho = 1.06 \times 10^3$ kg/m^3. Additionally, the electrodynamic width K is defined as the ratio of half-height H of the microchannel to the EDL thickness κ^{-1}. In the following calculations, all computed results are concerned with the steady status and the initial condition can be given by small arbitrary non-constant distribution.

Firstly, the numerical solutions of dimensionless rotating EOF velocity profiles computed from Eqs. (22) and (23) are compared with those of the analytical solution obtained by Chang and Wang [20] in Fig. 2 and related data are listed in Table 1, where $U_{eo} = -\varepsilon E\psi_w/\eta$. To ensure accuracy of the computed numerical solution, the numerical solution computed in present work is then compared with analytical results presented by Zhao et al. [32] in Fig. 3 and related data are listed in Table 2, where U_{avg} is the mean EOF velocity of Newtonian fluid without rotation. It is shown from Figs. 2 and 3, Tables 1 and 2 that they are agreed well with each other. Therefore, the present numerical method constructed above is valid and can be used to compute the rotating EOF velocity profiles of power-law fluid when $n \neq 1$.

Table 2
Comparison of analytical solutions in Ref. [32] with present numerical solutions.

u/U_{avg}			
z/H	Analytical solution (u_A)	Present numerical solution (u_N)	Relative error $\lvert(u_A - u_N)/u_A\rvert$
0	1.1110	1.0906	0.0184
0.1	1.1110	1.0906	0.0183
0.2	1.1107	1.0904	0.0183
0.3	1.1101	1.0898	0.0182
0.4	1.1084	1.0882	0.0182
0.5	1.1036	1.0836	0.0181
0.6	1.0908	1.0711	0.0180
0.7	1.0558	1.0369	0.0179
0.8	0.9607	0.9438	0.0176
0.9	0.7024	0.6905	0.0169
1	0	0	0

The variations of the numerical dimensionless rotating EOF velocity for different fluid behavior index n (0.7, 0.8, 1, 1.2, 1.5) are illustrated in Fig. 4. Similar to the results obtained by Vasu and De [33], when the angular velocity $\Omega = 0$, the velocities in x direction increase with the decrease of the power-law behavior index n. Their shapes more approximate to plug-like EOF velocity profiles for pseudoplastic ($n < 1$), and more approximate to parabolic velocity profile for $n > 1$. When the fluid is rotating in Fig. 4, an obvious feature of the velocity profiles in x direction is the steep velocity gradient and larger velocity magnitude near the wall. The reason is that the viscosity of power-law fluids depends on position across the channel. At the center of the microchannel, the velocity in x direction [see Fig. 4(a)] becomes concave both for pseudoplastic fluid ($n < 1$) and for dilatant fluid ($n > 1$) due to the effect of rotation. Besides, from Fig. 4(b), the velocity v in y direction remains nearly parabolic and its magnitude reduces with the power-law behavior index n.

The impacts of the rotating angular velocity Ω on dimensionless velocity both in x and in y directions are shown in Figs. 5 and 6 when the fluid behavior index $n = 0.8$ and $n = 1.2$ respectively. It can be seen from Figs. 5(a) and 6(a) that the velocity profiles are similar to the results in Vasu and De [33] if the rotating effect is ignored. The velocity in x direction decreases with the rotating angular velocity Ω both for $n = 0.8$ and for $n = 1.2$. From the point of view of mechanical balance, in the middle portion of the channel, the shear stress

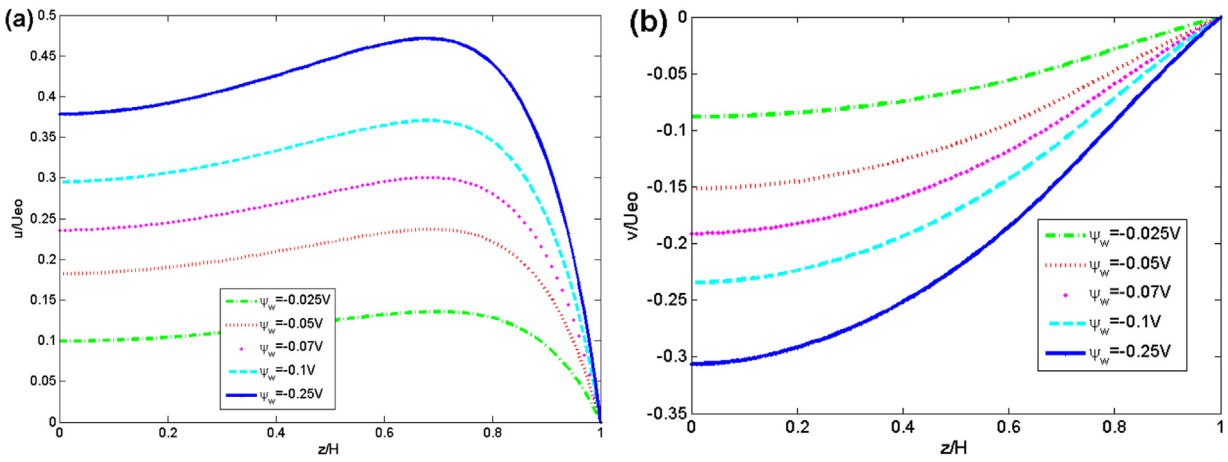

Fig. 10. The variations of the rotating EOF velocity with zeta potential, ψ_w ($n = 1.2$, $\Omega = 100$ rad/s, $K = 10$). (a) Dimensionless velocity u in x direction. (b) Dimensionless velocity v in y direction.

changes slowly and the electric field force has little effect, thus the Coriolis force plays the dominant role. It can be found from Figs. 5(b) and 6(b) that, Similar to Chang and Wang [20], the center velocities in y direction are reduced for high rotating velocity Ω. The velocity v behaves oscillating characteristic with reduced magnitude as the angular velocity Ω is further increased. Furthermore, the center velocity even becomes negative for the higher angular velocity Ω and a critical Ω can be determined. For pseudoplastic fluids, it can be found that when the K increases the critical Ω is almost unchanged from Fig. 5(a), (c) and (d) for prescribed zeta potential. However, from Fig. 5(a), (e) and (f), the critical Ω decreases with the zeta potential for given K. For dilatant fluids, the K has little influence on the critical Ω from Fig. 6(a), (c) and (d). However, for given K, the critical Ω increases with zeta potential from Fig. 6(a), (e) and (f).

Figs. 7 and 8 are plotted to show the effect of electrodynamic width K on rotating EOF velocity when $n = 0.8$ and $n = 1.2$ respectively. Similar to previous published literature, Large K leads to large rotating EOF velocity in x direction within the EDL near the wall [see Figs. 7(a) and 8(a)]. The velocity increases as the increasing K for pseudoplastic fluid ($n < 1$) as one moves away from the slit wall, but for dilatant fluid ($n > 1$) the velocity decreases with K. In addition, from Fig. 7(b) the velocity v in y direction displays a bowl-like shape and its magnitude increases with K when $n = 0.8$. The velocity v in y direction displays a parabolic shape and decreases with K when $n = 1.2$.

The impacts of the zeta potential on dimensionless velocity both in x and in y directions are shown in Figs. 9 and 10 when the fluid behavior index $n = 0.8$ and $n = 1.2$ respectively. It can be seen from Figs. 9(b) and 10(b) that the velocity in x direction increases in a region near to the microchannel wall and then attains the maximum value for both pseudoplastic and dilitant fluid. The minimum value of the velocity can be found at the center of the channel. Besides, we find the magnitude of the fluid velocity increase with the wall zeta potential no matter when $n = 0.8$ or when $n = 1.2$. The reason is that the high zeta potential could produce the larger electric field force near the EDL region and the larger velocity could be established outside the EDL region due to the viscosity of the fluid. It still can be found from Figs. 9(b) and 10(b) that the magnitude of the velocity in y direction is similar to the velocity in x direction.

5. Conclusions

We have presented a numerical study of the rotating EOF of power-law fluids in a slit microchannel at high zeta potential, where the charge density distribution was based on the nonlinear Poisson–Boltzmann equation. It is observed that the pseudoplastic has higher velocity in microchannel than that of dilitant for same operating conditions. Then the modified Cauchy momentum equations are computed numerically by the finite difference method. Computational results show that both power-law behavior index n, rotating angular velocity Ω and the wall zeta potential ψ_w play an important role in the rotating EOF velocity. Due to the rotating effect, the velocity profiles in x direction become steep near the wall. However, at the center of the microchannel, the velocity becomes concave both for pseudoplastic fluid ($n < 1$) and for dilatant fluid ($n > 1$). In a rotating system, aside from centrifugal force, the effect of the Coriolis force on fluid flow is important. The Coriolis force has an obvious effect at the center of the channel especially for large rotating angular velocity and it even alters the velocity direction. Moreover, the center velocity even becomes negative for the higher angular velocity Ω and a critical Ω can be determined. The critical Ω is almost unchanged for prescribed zeta potential both for pseudoplastic fluid ($n < 1$) and for dilatant fluid ($n > 1$). However, the critical Ω (about 600 rps) for dilatant fluid is higher than that of pseudoplastic fluid (about 400 rps). For given K, the critical Ω decreases with the zeta potential for pseudoplastic fluid and increases with zeta potential for dilatant fluid. Besides, we find that the higher wall zeta potential can facilitate transport for both pseudoplastic and dilitant fluid. This understanding helps in efficient design of fluid flow in a rotating microfluidic device which has applications in site specific species transport such as drug delivery and species separation. Also the main purpose of this research is to allow the designer to use the second law of the thermodynamics efficiently in calculation of rotating microfluidic systems.

Acknowledgements

The work was supported by the National Natural Science Foundation of China (Nos. 11062005 and 11202092), the Program for Young Talents of Science and Technology in Universities of Inner Mongolia Autonomous Region (No. NJYT-13-A02), Opening fund of State Key Laboratory of Nonlinear Mechanics, Research Program of science and technology at Universities of Inner Mongolia Autonomous Region (No. NJZY14109).

References

[1] H.A. Stone, A.D. Stroock, A. Ajdari, Engineering flows in small devices: microfluidics toward a lab-on-a-chip, Annu. Rev. Fluid Mech. 36 (2004) 381–411.

[2] D. Erickson, D. Li, Integrated microfluidic devices, Anal. Chim. Acta 505 (2004) 11–26.
[3] J.H. Masliyah, S. Bhattacharjee, Electrokinetic and Colloid Transport Phenomena, John Wiley & Sons Inc. Press, Hoboken, NJ, 2006.
[4] D. Burgreen, F.R. Nakache, Electrokinetic flow in ultrafine capillary slits, J. Phys. Chem. 68 (1964) 1084–1091.
[5] S. Levine, J.R. Marriott, G. Neale, N. Epstein, Theory of electrokinetic flow in fine cylindrical capillaries at high zeta potentials, J. Colloid Interface Sci. 52 (1975) 136–149.
[6] C.L. Rice, R. White, Electrokinetic flow in a narrow cylindrical capillary, J. Phys. Chem. 69 (1965) 4017–4023.
[7] H.K. Tsao, Electroosmotic flow through an annulus, J. Colloid Interface Sci. 225 (2000) 247–250.
[8] Y.J. Kang, C. Yang, X.Y. Huang, Electroosmotic flow in a capillary annulus with high zeta potentials, J. Colloid Interface Sci. 253 (2002) 285–294.
[9] Y.J. Jian, L.G. Yang, Q.S. Liu, Time periodic electro-osmotic flow through a microannulus, Phys. Fluids 22 (2010) 042001.
[10] C. Yang, D. Li, Analysis of electrokinetic effects on the liquid flow in rectangular microchannel, Colloids Surf. A: Physicochem. Eng. Asp. 143 (1998) 339–353.
[11] C. Yang, D. Li, J.H. Masliyah, Modeling forced liquid convection in rectangular microchannels with electrokinetic effects, Int. J. Heat Mass Transf. 41 (1998) 4229–4249.
[12] S. Arulanandam, D. Li, Liquid transport in rectangular microchannels by electroosmotic pumping, Colloids Surf. A: Physicochem. Eng. Asp. 161 (2000) 89–102.
[13] J. Pedlosky, Geophysical Fluid Dynamics, Springer Press, New York, 1987.
[14] B. Cushman-Roisin, Introduction to Geophysical Fluid Dynamics, Prentice Hall Press, New York, 1994.
[15] E.J. Hopfinger, P.F. Linden, The effect of background rotating on fluid motions: a report on Euromech 245, J. Fluid Mech. 211 (1990) 417–435.
[16] D.C. Duffy, H.L. Gillis, J.L.N.F. Sheppard, G.J. Kellogg, Microfabricated centrifugal microfluidic systems: characterization and multiple enzymatic assays, Anal. Chem. 71 (1999) 4669–4678.
[17] M. Takashima, The effect of rotation on electrohydrodynamic instability, Can. J. Phys. 54 (1976) 342–347.
[18] M.I.A. Othman, Electrohydrodynamic instability of a rotating layer of a viscoelastic fluid heated from below, Z. Angew. Math. Phys. 55 (2004) 468–482.
[19] A.C. Ruo, M.H. Chang, F. Chen, Effect of rotation on the electrohydrodynamic instability of a fluid layer with an electrical conductivity gradient, Phys. Fluids 22 (2010) 024102.
[20] C.C. Chang, C.Y. Wang, Rotating electro-osmotic flow over a plate or between two plates, Phys. Rev. E 84 (2011) 056320.
[21] D. Dutta, Transport of charged samples in fluidic channels with large zeta potentials, Electrophoresis 28 (2007) 4552–4560.
[22] B.J. Kirby, E.F. Hasselbrink Jr., Zeta potential of microfluidic substrates: 1. Theory, experimental techniques, and effects on separations, Electropheresis 25 (2004) 187–202.
[23] B.J. Kirby, E.F. Hasselbrink Jr., Zeta potential of microfluidic substrates: 2. Data for polymers, Electrophoresis 25 (2004) 203–213.
[24] A. Elazhary, H.M. Soliman, Analytical solutions of fluid flow and heat transfer in parallel-plate micro-channels at high zeta-potentials, Int. J. Heat Mass Transf. 52 (2009) 4449–4458.
[25] P. Dutta, A. Beskok, Analytical solution of combined electroosmotic/pressure driven flows in two-dimensional straight channels: finite Debye layer effects, Anal. Chem. 73 (2001) 1979–1986.
[26] W.J. Luo, Y.J. Pan, R.J. Yang, Transient analysis of electro-osmotic secondary flow induced by dc or ac electric field in a curved rectangular microchannel, J. Micromesh. Microeng. 15 (2005) 463–473.
[27] M.S. Chun, Electrokinetic secondary-flow behavior in a curved microchannel under dissimilar surface conditions, Phys. Rev. E 83 (2011) 036312.
[28] Q.S. Liu, Y.J. Jian, L.G. Yang, Alternating current electroosmotic flow of the Jeffreys fluids through a slit microchannel, Phys. Fluids 23 (2011) 102001.
[29] Q.S. Liu, Y.J. Jian, L.G. Yang, Time periodic electroosmotic flow of the generalized Maxwell fluids between two microparallel plates, J. Non-Newton. Fluid Mech. 166 (2011) 178–186.
[30] Y.J. Jian, Q.S. Liu, L.G. Yang, AC electroosmotic flow of generalized Maxwell fluids in a rectangular microchannel, J. Non-Newton. Fluid Mech. 166 (2011) 1304–1314.
[31] S. Das, S. Chakraborty, Analytical solutions for velocity, temperature and concentration distribution in electroosmotic microchannel flow of a non-Newtonian bio-fluid, Anal. Chim. Acta 559 (2006) 15–24.
[32] C. zhao, E. Zholkovskij, J.H. Masliyah, C. Yang, Analysis of electroosmotic flow of power-law fluids in a slit microchannel, J. Colloid Interface Sci. 326 (2008) 503–510.
[33] N. Vasu, S. De, Electroosmotic flow of power-law fluids at high zeta potentials, Colloid Surf. A: Physicochem. Eng. Asp. 368 (2010) 44–52.
[34] R.B. Bird, R.C. Armstrong, O. Hassager, Dynamics of Polymeric Liquids, Fluid Mechanics, vol. 1, second ed., Wiley-Interscience Press, 1987.
[35] W.B. Russel, D.A. Saville, W.R. Schowalter, Collodial Dispersions, Cambridge University Press, Cambridge, 1992.